



Graphene kirigami as reinforcement and interfacial bonding effect for toughness and strength of silicon-based nanocomposites



Yafei Wang^{a,b}, Changguo Wang^{a,b,*}, Yunce Zhang^{a,c}, Huifeng Tan^{a,b}

^a Center for Composite Materials, Harbin Institute of Technology, Harbin 150001, PR China

^b National Key Laboratory of Science and Technology on Advanced Composites in Special Environments, Harbin Institute of Technology, Harbin 150080, PR China

^c College of Aerospace and Civil Engineering, Harbin Engineering University, Harbin 150001, PR China

ARTICLE INFO

Keywords:

Graphene kirigami
Toughness
Strength
Interfacial bonding strength
Nanocomposite

ABSTRACT

This paper studies the toughness, strength and interfacial bonding effect of graphene kirigami silicon-based nanocomposite (GKSN) using molecular dynamics (MD) simulation. The GKSN model is proposed based on a hybrid potential. It is found that the toughness and maximum strength of GKSN are related to the number of interior cuts and density of kirigami patterns for graphene kirigami. Mechanical response of GKSN has four typical stages, including initial wrinkling, linear increasing, ratcheting and failure. Locking effect can significantly enhance the toughness and maximum strength of GKSN with some rare expectations. With increasing interfacial bonding strength of GKSN, toughness and maximum strength increase steadily. Finally, two novel nanocomposites based on graphene kirigami can be designed. The obtained results in this paper can provide a fundamental understanding of the maximum strength and an insight for enhancing the toughness of graphene kirigami nanocomposite. The proposed mechanisms may have general significances for the design of the next generation “super-tough” and “super-strong” nanocomposites.

1. Introduction

Composites incorporating nanosized carbon reinforcements have become increasingly important for the next generation “super-tough” and “super-strong”, enabling a combination of mechanical and physical properties unattainable in traditional polymers, metals and ceramics [1–4]. There is great need to expand the design space for accessible toughness and strength and exploit a manageable set of design paradigms especially for performance enhancements of multipotent brittle materials. Mechanically, failure of brittle and stiff materials highly depends on micro- and nano-defect distributions, which trigger further propagation of cracks, leading to complete fracture [5,6]. Typically, it is advisable to arrest the propagation of nanocracks by combining hard and soft components, such as Al matrix nanocomposites reinforced by graphene nanoplatelets [7,8], but the mechanism of their interfacial adhesion for nanocomposites can be hard to theoretically predict and experimentally observe owing to the complexity of deformation and scale limitation with respect to components.

On the other hand, as every coin has two sides, defects in reinforcements could be engineered to realize certain exciting properties by introducing the concept from the art of paper kirigami due to the rapid development of manufacturing techniques (such as

photolithography, sonochemical method, thin etching, templated growth and self-assembly) [9–13]. Several pioneering experiments have been carried out on nanocomposites incorporating reinforcement with kirigami pattern to characterize their mechanical response and showcase the widely physical application. Based on top-down patterning techniques, Shyu et al. [3] used kirigami patterned graphene oxide (GO)/PVA to characterize the significant enhancement of ultimate strain from 4 to 370%, which the mechanical behaviors of kirigami nanocomposites can be accurately predicted through finite element methods. Using scanning electron microscopy (SEM), the unique properties of kirigami nanocomposites as plasma electrodes were characterized, which can open up a wide range of novel technological solutions for stretchable electronics and optoelectronic devices. Subsequently, Guan et al. [2] studied the mechanical properties of free-standing nanoconfined kirigami polymer nanosheet with SEM and atomic force microscopy (AFM) and observed a remarkable mechanical reversibility under more than 1000 cycle durability tests with 2000% deformation. Lyu et al. [14] used silver nanoparticles/aramid nanofiber matrix nanocomposite with kirigami pattern to observe the high stretchability. More recently, Xu et al. [15] studied the mechanical and optical properties of kirigami nanocomposites as wide-angle diffraction gratings under uniaxial stretching and showed that the kirigami pattern

* Corresponding author at: Center for Composite Materials, Harbin Institute of Technology, Harbin 150001, PR China.
E-mail address: wangcg@hit.edu.cn (C. Wang).

can reduce the strain by 2 orders of magnitude for stretching deformation, enabling reconfigurable optical gratings with over a 100% range of period tunability. Despite the latest scientific advances have provided extremely important information on the observed mechanical response of kirigami nanocomposites, detailed physical insights into atomic-level deformation mechanisms have not been investigated.

To initiate the theoretical analysis and provide the fundamental physical insights into the origins of enhanced mechanical properties, in this work we investigate a diamond matrix with graphene kirigami model.

It is well known that ceramics are attracting widespread interest in fields such as electronic, industrial, space, automotive and defense applications, resulting from their high strength, stiffness and stability of high temperature. However, the brittle nature of monolithic ceramics restricts their use. To address this problem, a lot of literature in the proceedings are explicitly devoted to fibre-based ceramic composites. And much research has been focused on CNT reinforced ceramic composites [16] in regard to the enhancement of toughness [17], strength [18], electrical conductivity [19] and thermal conductivity [20]. Especially, for CNT reinforced silicon matrix composites, Chen et al. [21] reported the significant improvement of fracture toughness and maximum strength as compared with that of monolithic silicon using molecular dynamics (MD) simulation. Graphene, as a wonderful two-dimensional material, has the similar mechanical and physical properties compared to CNT. The stiffness and tensile stiffness are separately as large as 100 GPa and 1 TPa [22]. While the advantages of using graphene as reinforcement over CNTs are the larger surface area as well as the lower tangle tendency. It means that graphene can be easily dispersed into a matrix. On the contrary, surface modification of CNT is always used to disperse them. Therefore, by considering these excellent properties and advantages, dispersing graphene into ceramics matrix as the multifunctional composites has great application potential. Graphene kirigami has been proposed in experiments and it showcases the significantly flexible mechanical properties. The toughness, strength and physical properties of graphene kirigami can be adjusted by excising different kirigami motifs [23]. Moreover, topological surface of graphene kirigami under tension due to lateral buckling can contribute to additional unique electrical and thermal properties [24,25]. The kirigami technology is useful to enhance the ductility, toughness and change the brittle nature of graphene. The graphene kirigami with specific periodic motifs has large fracture strain, which can be up to three times larger than that of graphene nanoribbon base on MD simulation [26]. Unfortunately, to the best of our knowledge, it appears that there has been only limited research into the mechanical performance of graphene ceramic matrix composites and graphene kirigami ceramic matrix composites, and it is especially true that little work has been done on the problem of interfacial bonding effect of graphene kirigami ceramic matrix composites. In order to guide the design of multifunctional ceramics in future applications, further study is necessary and significant in the graphene/graphene kirigami ceramic matrix composites.

Research on graphene/graphene kirigami ceramic matrix composites, although promising, is still quite unexploited. The purpose of this research is to give a fundamental investigation of mechanical properties of pristine graphene silicon-based nanocomposite (PGSN) and graphene kirigami silicon-based nanocomposites (GKSN) using MD simulation, in which Si is a representative ceramic matrix. The structure of this paper is organized as follows. Section 2 describes the computational methods and establishes simulation models based on two independent dimensionless parameters. Section 3 is devoted to the discussion of mechanical properties of GKSN, and the comparison of toughness and maximum strength for GKSN and PGSN. Moreover, toughening mechanism, interfacial bonding effect, temperature impact and novel nanocomposite design of GKSN are also provided in this section. Section 4 gives concluding remarks.

2. Computational methods and model

Classical molecular dynamics (MD) simulation in current research was based on the large-scale atomic/molecular massively parallel simulator (LAMMPS) developed by Sandia National Laboratories [27]. Hybrid potential and periodic boundary conditions were designated to establish the silicon-based nanocomposites. To best capture the mechanical response of silicon-based nanocomposites and interfacial bonding effect, the Erhart/Albe-Tersoff potential was applied to describe interactions from Si-Si atoms and C-Si atoms, the adaptive intermolecular reactive empirical bond order (AIREBO) potential was used to define the interactions of C-C atoms, the hybrid potential for this work were adjusted as in Refs. [8,21,28,29]. Therefore, the potential energy stored in the system can be directly expressed as

$$E_{\text{Total}} = E_{\text{Si}}^{\text{Tersoff}} + E_{\text{C}}^{\text{AIREBO}} + E_{\text{C-Si}}^{\text{Tersoff}} \quad (1)$$

The Erhart/Albe-Tersoff potential is a modified version of Tersoff and can be written as follows

$$E^{\text{Tersoff}} = \sum_{i>j} f_C(r_{ij})[V_R(r_{ij}) - b_{ij}V_A(r_{ij})] \quad (2)$$

where $V_R(r_{ij})$ and $V_A(r_{ij})$ represent the interatomic repulsions and attractions, separately. b_{ij} , bonding strength, is a key factor and it can describe the many-body effect, $f_C(r_{ij})$ is the smooth cut-off function, based on which the interaction of two atoms can approach zero smoothly. Information on the relevant functions is available in Ref. [30]. It is important to note that in current research, the weakest bonding strength $\varepsilon = 0.01$ eV is designated to investigate the interfacial bonding effects described by Lennard-Jones (LJ) potential while the Tersoff potential is used to simulate the maximum bonding strength. This technique is according to Refs. [21,31–34].

The adaptive intermolecular reactive empirical bond order (AIREBO) potential [35] consists of three sub-potentials and it can be expressed as a summation of Lennard-Jones potential, the torsional potential and the reactive empirical bond order (REBO) potential:

$$E^{\text{AIREBO}} = \frac{1}{2} \sum_i \sum_{j \neq i} \left[E_{ij}^{\text{LJ}} + \sum_{k \neq i,j} \sum_{l \neq i,j,k} E_{ijkl}^{\text{TORSION}} + E_{ij}^{\text{REBO}} \right] \quad (3)$$

where the E_{ij}^{REBO} term from the REBO potential based on Ref. [36] can be calculated as

$$E_{ij}^{\text{REBO}} = f(r_{ij})[V_{ij}^R + b_{ij}V_{ij}^A] \quad (4)$$

where V_{ij}^R is the repulsion term and V_{ij}^A is the attraction term, b_{ij} is the bond order term between atoms which can activate attraction term for bonded atoms. $f(r_{ij})$ is the cut-off function and it can limit the interatomic interactions of the nearest atoms. Additionally, for the cutoff distance of REBO force field, it should be adjusted to 0.2 nm to avoid the spurious strengthening effect.

In models of graphene kirigami silicon-based nanocomposites (GKSN) for tension simulation, the initial equilibrium is firstly performed by relaxing the system for 150 ps and the Berendsen thermostat (with NVE (constant number of particles, constant volume, and constant energy) ensemble) is employed with a target temperature 10 K. Standard velocity-Verlet time integration with the timestep of 1 fs is designated to solve the motion equations. To validate the efficiency of equilibration time, a specific model with 200 ps is carried out at 10 K. Obtained equilibrated geometry is almost the same as the 150 ps equilibration. Thus, the equilibration time of 150 s is applied to all subsequent GKSN to avoid the time consuming. Here, the low temperature of 10 K is used to eliminate thermal perturbation for tension tests, while the effects of temperature on toughness and strength of GKSN are suitably investigated in Section 3. After the initial equilibrium, tensile displacements in the length direction of Si matrix is performed base on the laterally periodic boundary conditions. The velocity of 0.1 Å/ps is applied on the left end, and the other end is

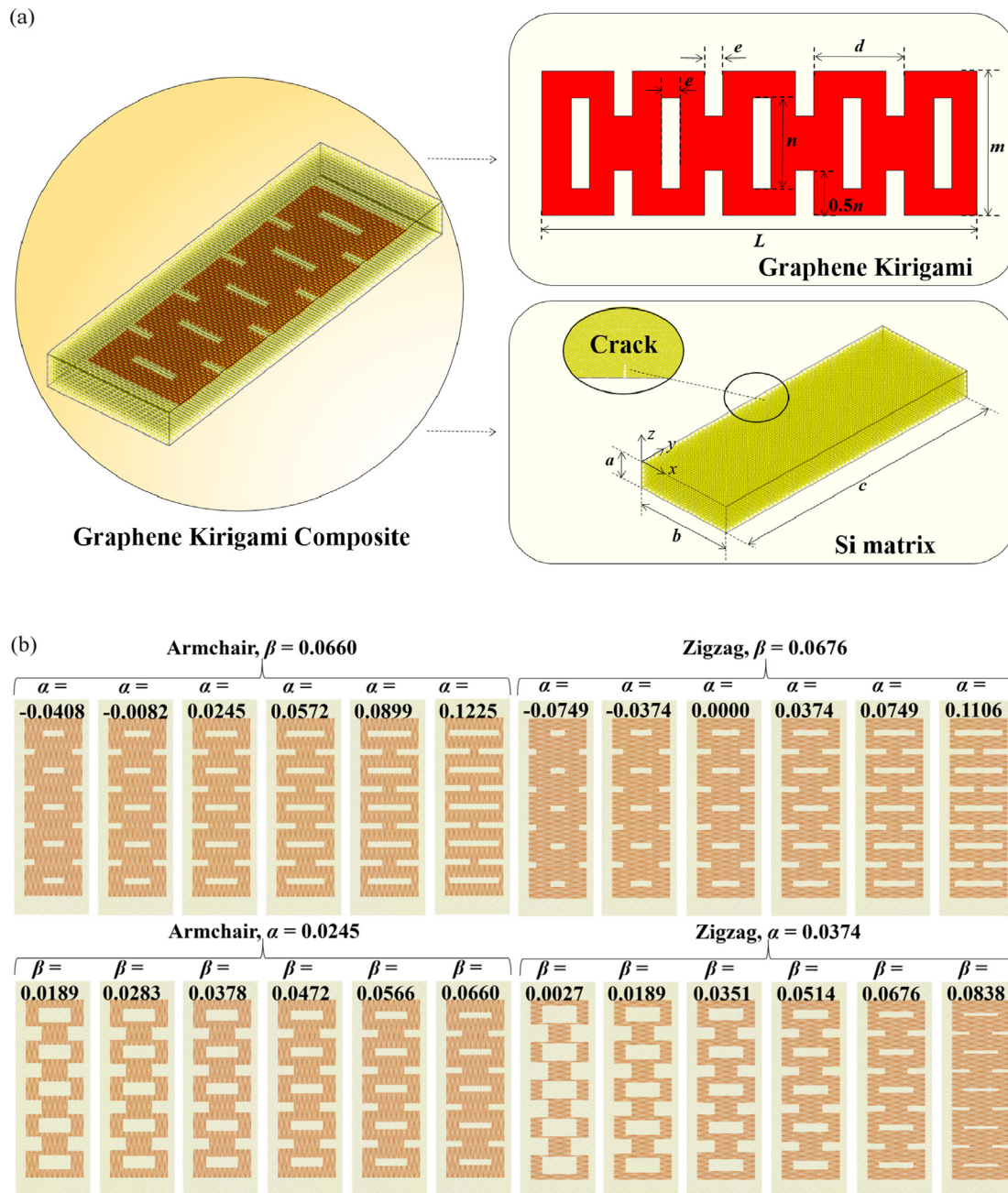


Fig. 1. (a) Schematic of graphene kirigami silicon-based nanocomposites (GKSN) with the key geometric parameters. (b) schematic of GKSN described by two independent dimensionless parameters (α , β) and chiralities (armchair, zigzag).

designated as a velocity of $-0.1 \text{ \AA}/\text{ps}$. The corresponding strain rate of tensile process is 0.000635 ps^{-1} . Stain rates of $o(0.001 \text{ ps}^{-1})$ have been demonstrated to give results which include negligible dynamic effects in graphene nanoribbons [37]. Therefore, the strain rate effects (dynamic effects) are insignificant. To ensure that $0.02 \text{ nm}/\text{ps}$ is a proper velocity, one MD simulation is run with $0.002 \text{ nm}/\text{ps}$ at 10 K . The corresponding results are very similar to that from the $0.02 \text{ nm}/\text{ps}$ simulation. After the fracture of GKSN, the relevant physical parameters can be collected and visualized by OVITO software.

Virial theory is used to calculated the stress of GKSN, and the virial stress can be expressed as

$$(\sigma_{GKSN})_{\mu\nu} = \frac{1}{V} \left[\sum_{i=1}^N m v_\mu^i v_\nu^i + \frac{1}{2} \sum_{i=1}^{N-1} \sum_{j=i+1}^N r_{ij,\mu} F_{ij,\nu} \right] \quad (5)$$

where V is the total volume of the system, μ and ν are the components

in the Cartesian coordinate, m is the mass of atom i , v_μ^i is the velocity of μ component for atom i , $r_{ij,\mu}$ is the distance between atom i and j for the μ component, and $F_{ij,\nu}$ is the interatomic force between atom i and atom j for ν component.

A representative GKSN unit cell and its geometry parameters can be seen in Fig. 1(a). The key geometric parameters include: the length of kirigami graphene L , the width of kirigami graphene m , the length of interior cut n , the width of interior cut e and the distance between two interior cuts d . While the total size of GKSN unit cell is fixed at a constant $a \times b \times c = 27 \text{ \AA} \times 109 \text{ \AA} \times 315 \text{ \AA}$. A vacancy in Si matrix is introduced to accommodate the graphene kirigami as the reinforcement. A crack was initiated at the edge of the silicon matrix for controlling the direction of crack propagation [34], this process is based on the Refs. [21,34]. The interface average distance between Si and C is designated as 1.95 \AA , which is similar to the average distance used in

Refs. [8,21,34]. This is because if the distance of two atoms is less than 1.95 Å the SiC covalent bond can be formed, and van der Waals interaction will be identified when the average distance between Si and C exceeds 1.95 Å. As the current research intends to provide a full understanding of geometry-dependent toughness and strength of GKS, a series of GKS unit cells are proposed and systematically summarized in Fig. 1(b) based on two independent dimensionless parameters [26] and chiralities (armchair, zigzag). α represents the ratio between interior overlapping cut length and the kirigami graphene length, it directly affects the number of interior cuts and can be written as

$$\alpha = (2n - m)/2L \quad (6)$$

β is the ratio of overlapping width to graphene kirigami length, it describes the density of kirigami patterns and can be expressed as

$$\beta = (d - 2e)/2L \quad (7)$$

So far, the computational details and model development have been thoroughly demonstrated, further analysis will be systematically performed, as we provided in Section 3.

3. Results and discussion

3.1. Overview of mechanical properties for GKS

Fig. 2 summarizes the effects of two dimensionless parameters (α and β) on the toughness, maximum strength and tensile modulus of GKS based on chirality differences and Eqs. (6)–(7). Toughness $U_{Toughness}$ is calculated as follows

$$U_{Toughness} = \int_0^{\varepsilon_{cf}} \sigma d\varepsilon \quad (8)$$

where ε_{cf} represents the strain when GKS is complete rupture under tension. And the red line is designated to describe the variation of toughness for GKS with different geometries and chiralities. The tensile modulus is obtained by using linear fitting technology, the first modulus due to initial wrinkling of graphene kirigami and the second modulus because of covalent bond formation are separately represented by the blue line and black line. Their specific definitions will be provided in next subsection. Fig. 2(a) and (b) demonstrate the effects of the ratio between the interior overlapping cut length and the kirigami graphene length α on toughness and tensile modulus of GKS with the similar β and different chiralities. In general, with the increasing of α , toughness tendencies of both armchair and zigzag chirality decline, which represent the restraint ability of crack growth gradually decreases. For tensile modulus, with increasing of α the first modulus and the second modulus monotonically decrease, while the second modulus is always larger than the first modulus. Additionally, for similar β the influence of chirality difference on the toughness and tensile modulus is not obvious. Fig. 2(c) and (d) shows that with increasing of the ratio of overlapping width to graphene kirigami length β the toughness and tensile modulus of GKS are increasing. With the density decreasing of kirigami cutting, the defects in kirigami graphene tend to become smaller, resulting in the increasing tendencies of the toughness and tensile modulus. However, it is surprising to find that for the same length and width of graphene, the results of toughness from pristine graphene silicon-based nanocomposite (PGS) are smaller than the toughness of GKS for several cases. The corresponding toughening mechanisms for relatively short graphene/graphene kirigami embedded in silicon-based nanocomposite are investigated in Section 3.2. Apart from that, the influence of α and β on the maximum strength of GKS by considering the chirality differences can be seen in Fig. 2(e) and (f), for both armchair and zigzag GKS, the maximum strength of GKS presents the decreasing tendency when α is increasing and β is decreasing. It is apparent that kirigami is an effective method to change the maximum strength and toughness of GKS. We also find the remarkable strength enhancement of GKS as compared with that of

PGS for some cases. It is important to note that for all cases in this section the interfacial bonding strength is designated as the maximum, in other words, the Tersoff potential function is used to describe the interfacial interactions between graphene kirigami and Si matrix.

3.2. Deformation responses and toughening mechanism

Fig. 3 reveals the deformation response and toughening mechanism of GKS, for some cases the simulation results of GKS are also compared with the pristine graphene silicon-based nanocomposite (PGS) and pure silicon. Fig. 3(a) shows the stress-strain curves of GKS for zigzag graphene kirigami with $\beta = 0.0676$, while the toughness, tensile modulus and maximum strength obtained from Fig. 3(a) are in accordance with the Fig. 2(b). As a demonstration, the GKS with $\beta = 0.0676$, $\alpha = -0.0374$ and zigzag chirality (for graphene kirigami) is designated to reveal the toughening mechanism. Fig. 3(b) provides comparisons of simulation results based on molecular dynamics corresponding to specific GKS, PGS and pure silicon with the same simulation environments and conditions. The stress-strain curves for GKS, PGS and pure silicon are respectively represented by red line, black line and blue line. Here, we start by investigating the deformation response of GKS. It is shown in Fig. 3(b) that the whole deformation process of GKS can be divided into four stages. Before the uniform tensile loading is applied, the initial equilibrium is performed as we can see from Fig. 3(c), and then tensile loading is applied on both ends to carry out the tension test as shown in the inset of Fig. 3(c). The initial equilibrium of GKS makes the graphene kirigami possible to be its wrinkling state as shown in Fig. 3(d). Due to mismatch of equilibrium size between graphene kirigami and Si matrix, the wrinkling effect of graphene kirigami will be aggravated. Once the tensile loading is increasing, the competition relationships between wrinkling graphene kirigami in GKS and de-wrinkling effect induced by tensile loading along the y-direction (see Figs. 1(a) and 3(c)) can result in a related low slope as we can see from the stage I of initial wrinkle, and we define the corresponding tension modulus of GKS as the first modulus. This effect can directly demonstrate the first modulus is always smaller than the second modulus. Here, we should note that the first modulus is originated from non-tangled graphene, that is, the average distance between Si matrix and graphene nanoplatelets. In this paper only constant initial average distance is used, a variable distance would be another possibility for further studies.

At the turning point of stage I and stage II, the wrinkle graphene kirigami turns to a flat state and starts to flip out of the plane. With the loading further increasing, the interior cut flipping is the main contribution to achieve the enhancement of stress. As shown in Fig. 3(e), in stage II of linear increasing, the interatomic force of interface between graphene kirigami and silicon experiences a transformation from van der Waals forces in stage I to covalent bonds in stage II. In Fig. 3(e), the typical geometric flipping effect and interfacial adhesion enhancement effect can qualitatively explain the key mechanism: yellow regions in the red rectangle represents the flipping-up regions of graphene kirigami and covalent bonds are formed by C atoms and upper Si atoms. Dark regions in the red rectangle represent the flipping-down regions of kirigami graphene, causing the formation of covalent bonds between C atoms and lower Si atoms. With the formation of covalent bonds in both ends of kirigami graphene, kirigami-induced locking effect due to geometric flipping becomes the main mechanism to realize the linear increase of stress, resulting in significant enhancement of toughness and maximum strength of GKS. To give an accessible explanation, the adhesion effect of octopus tentacles can supply an interesting analogy for locking effect due to geometric flipping of graphene kirigami in GKS.

Breaking of local covalent bonds occurs at the strain of 15%. This phenomenon can be reflected in stage III as shown in Fig. 3(f), which corresponds to the occurrence of “ratcheting” in stress-strain curves (see Fig. 3(b)). Breaking of covalent bonds mainly occurs at three

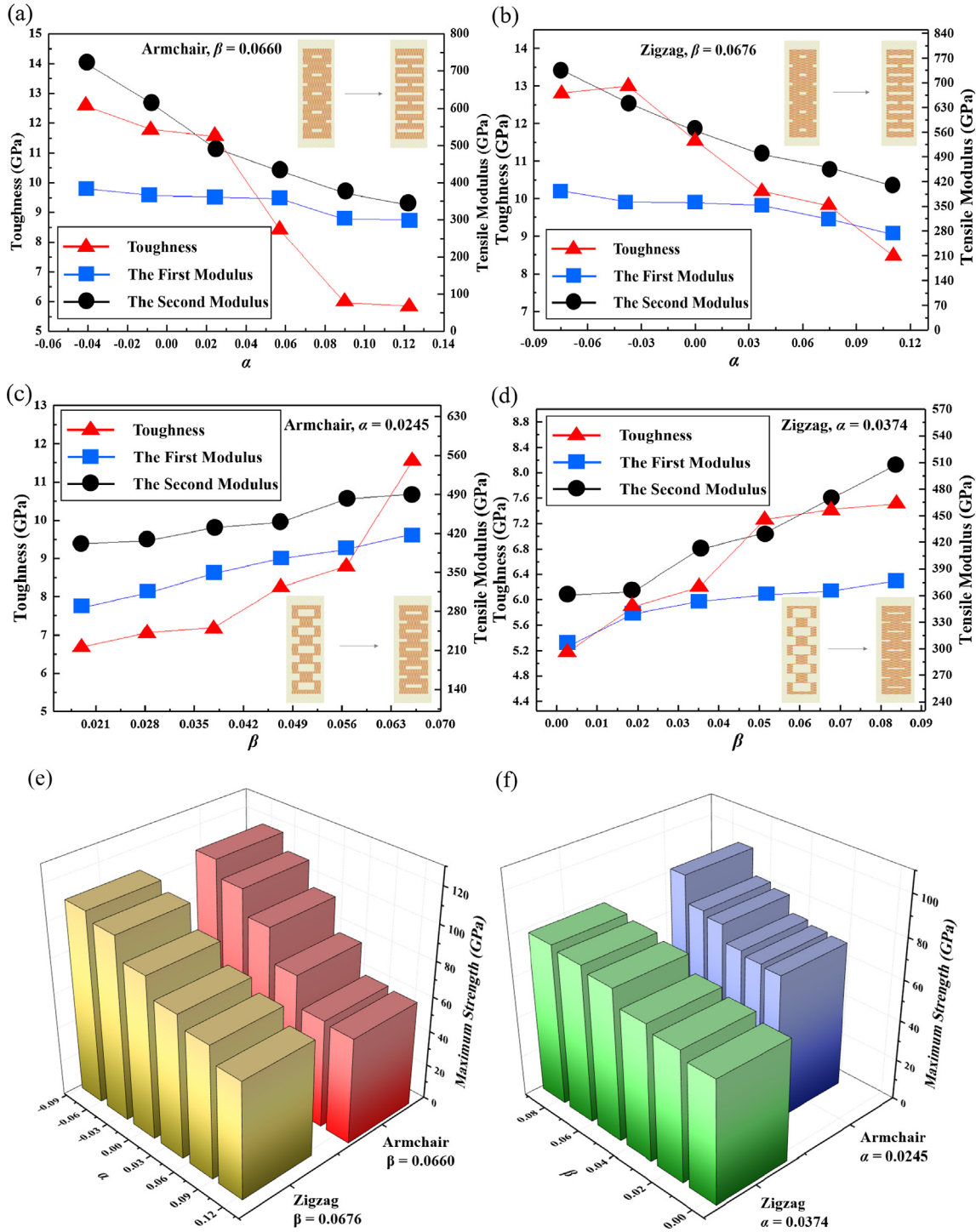


Fig. 2. (a) The effects of the ratio between the interior overlapping cut length and the kirigami graphene length α on toughness and tensile modulus of GKSН with the specific $\beta = 0.0660$ and armchair chirality of graphene kirigami. (b) The effects of α on toughness and tensile modulus of GKSН with the specific $\beta = 0.0676$ and zigzag chirality of graphene kirigami. (c) the effects of the ratio of overlapping width to graphene kirigami length β on toughness and tensile modulus of GKSН with the specific $\alpha = 0.0245$ and armchair chirality of graphene kirigami. (d) The effects of β on toughness and tensile modulus of GKSН with the specific $\alpha = 0.0374$ and zigzag chirality of graphene kirigami. (e) The effects of α on the maximum strength of GKSН with the different β and chiralities of graphene kirigami. (f) The effects of β on the maximum strength of GKSН with the different α and chiralities of graphene kirigami.

different regions, both ends of graphene kirigami, both sides of graphene kirigami along the x -direction and the flipping regions formed in stage II. Compared to reversible increasing of the first two stages, the stage III of “ratcheting” is a representation of ductility due to the breaking of covalent bonds. To some extent, the amount of “ratcheting” effect will influence the maximum strength and toughness of KGC.

In stage IV of failure for GKSН, failure process can be seen in

Fig. 3(g), and the toughness and maximum strength are respectively up to 13.1 GPa and 104.6 GPa. The bridging effect occurs at this stage, which is relative to the debonding and sliding effects between nano-sized graphene kirigami and ceramic matrix. The bridging effect can stabilize the crack by exerting closure traction and transfer sufficient load after first cracking to allow the ceramic matrix to undergo multiple cracking. Therefore, bridging effect will give a final contribution to

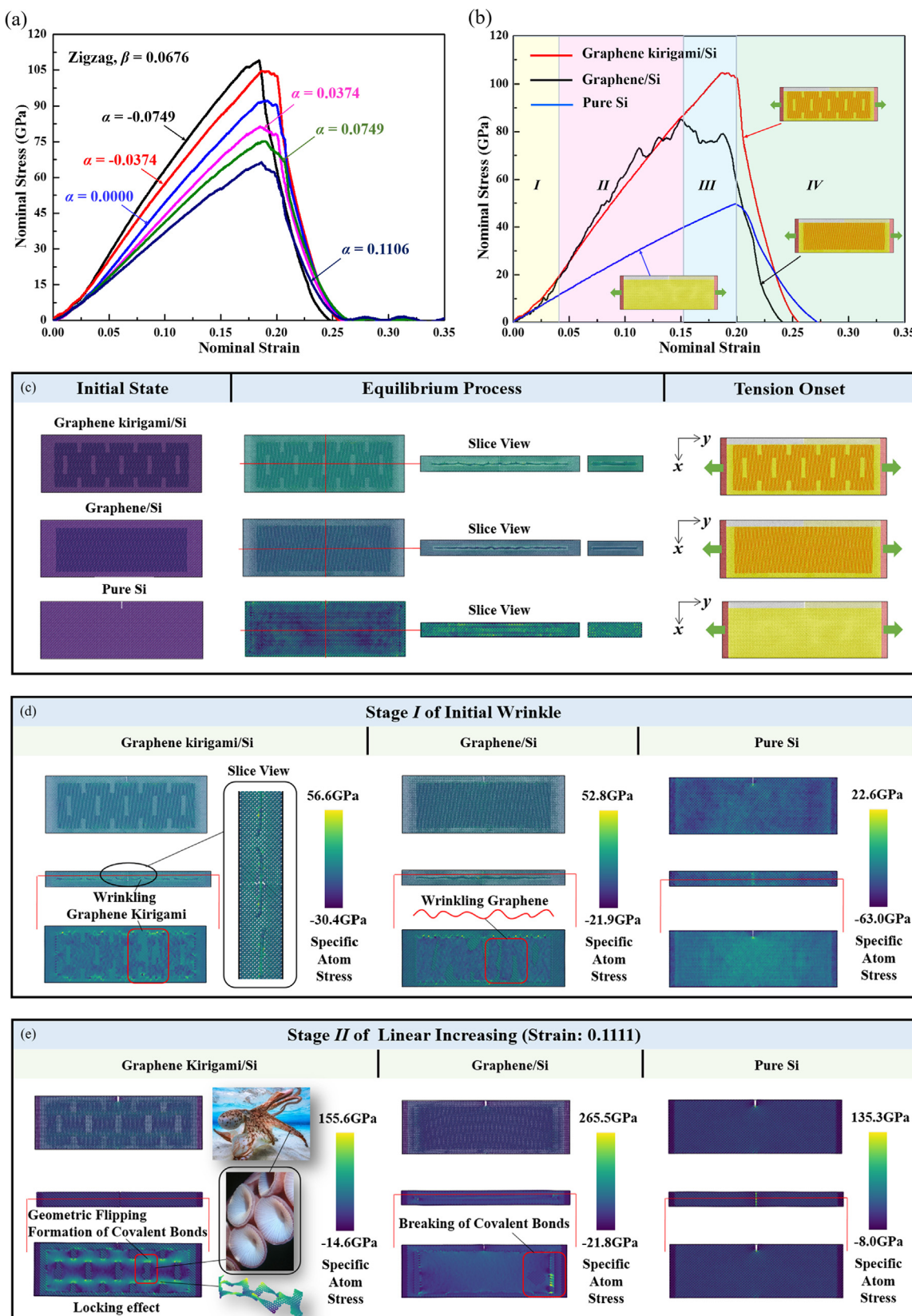


Fig. 3. (a) The stress-strain relation of GKSN with different α for zigzag graphene kirigami and $\beta = 0.0676$. (b) Comparison of stress-strain curves for GKSN, PGSN and pure Si material. (c) Model establishments of PGSN and pure Si and the initial state of MD simulation for GKSN, PGSN and pure Si material. (d) The stage I of the deformation process for GKSN. (e) the stage II of the deformation process for GKSN. The adhesion effect of octopus tentacles can supply an interesting analogy for locking effect due to geometric flipping of graphene kirigami in GKSN. (f) The stage III of the deformation process for GKSN. (g) The stage IV of the deformation process for GKSN. The deformation responses of PGSN and pure Si are also provided in (d)–(f). The color bar represents the specific atom stress.

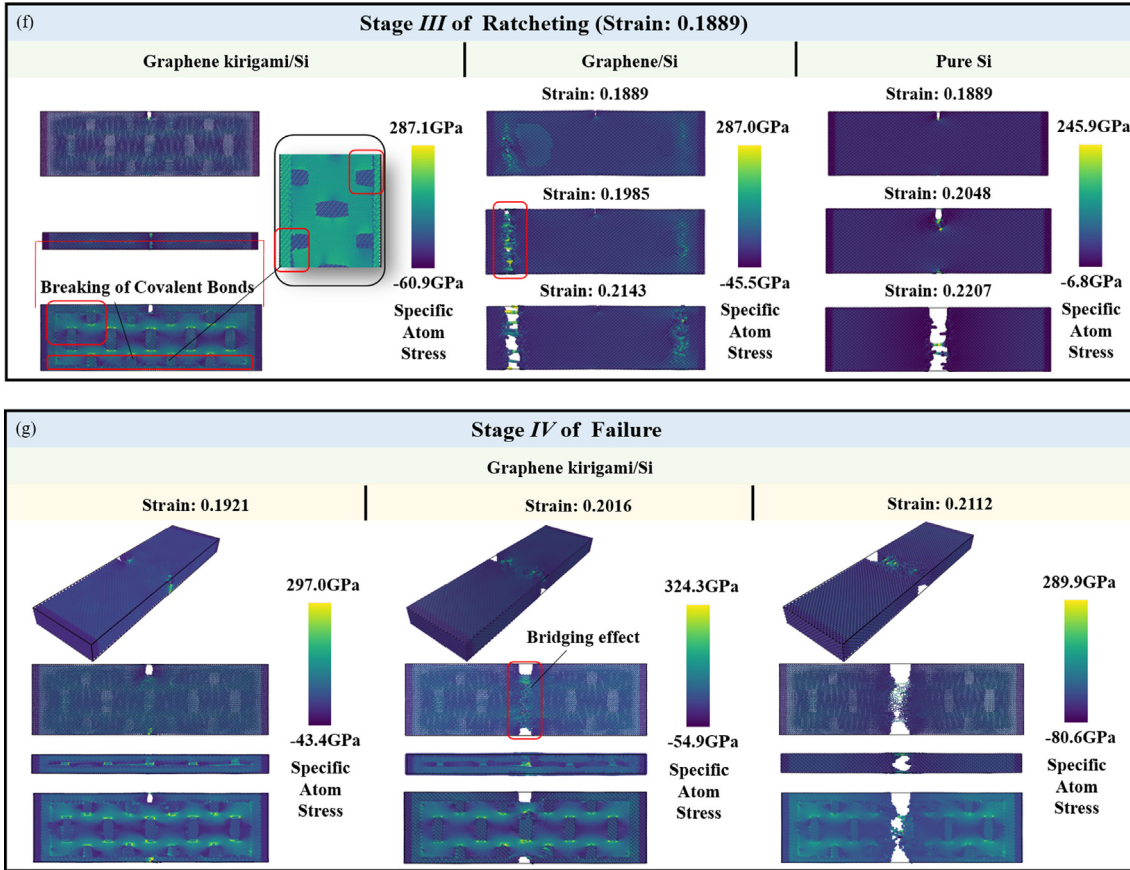


Fig. 3. (continued)

restrain the complete failure of GKS. The contribution of bridging effect on the toughness and maximum strength enhancement of graphene silicon-based nanocomposite (see Fig. 3(b)) are in accordance with previous experiments, such as toughening in graphene ceramic composites reported by Walker [38].

For systematicness, we also considered the nanostructures of pure silicon material and pristine graphene in Si matrix as illustrated by Fig. 3(b). Strikingly, results of MD simulation give a stress-strain of PGSN and pure silicon which the resulting toughness and maximum strength are both lower than the GKS. Especially, the maximum strength of GKS is increased by 23.1% and 110.3% as compared with that of PGSN and pure silicon material, separately. Toughness of pure silicon is 6.87 GPa, which is in line with previous experiments 6.9 GPa reported by Petersen [39]. The toughness of PGSN is 11.2 GPa based on MD simulation, and the toughness of GKS is increased by 16.9% and 90.2% as compared with that of PGSN and pure silicon material, respectively. These obtained results have demonstrated that graphene kirigami is an effective way to enhance the toughness and maximum strength of silicon matrix composites, while silicon is a typical brittle material.

Next, we briefly introduce the deformation process of PGSN and pure silicon material, and explain the reason of toughness and maximum strength enhancement for GKS. As seen in Fig. 3(c), defect-free graphene in PGSN also presents a wrinkling state in the stage of initial simulation (see Fig. 3(d)), so PGSN also has the first modulus. But the relatively short graphene nanoribbon has a smaller in-plane compliance, moreover, the mismatch of bonding strength for Si-C between interface and two ends is very large. The breaking of covalent bond for short graphene embedded in Si matrix will first occur at the two ends as detailed in Fig. 3(e), and then pristine graphene will be pulled out and form the bridging effect as shown in Fig. 3(f). However, for GKS the graphene kirigami can decrease its intrinsic in-plane stiffness and

geometric flipping supply the locking effect to enhance the interfacial adhesion. Therefore, for some cases graphene kirigami can obviously enhance the maximum strength and toughness of silicon-based nanocomposites. For pure silicon, it is a typical brittle material, the strain-to-rupture process can be seen in Fig. 3(c)–(f), and in this paper we have provided a reliable estimate of toughness for pure Si compared with previous literature.

3.3. Temperature impacts and interfacial bonding effect

Temperature always plays an important role in influencing the mechanical properties of nanocomposites. Here, we first investigate the toughness and maximum strength of GKS with $\beta = 0.0676$ and $\alpha = -0.0374$ for zigzag graphene kirigami under temperatures ranging from 10 K to 750 K. Fig. 4(a) illustrates the toughness and maximum strength of GKS at various temperatures. It is obvious that temperature exerts a significant influence on the mechanical response of GKS, resulting in severe decreasing in its toughness and maximum strength at the relatively high temperature. This indicates that large thermal perturbation can deteriorate the bonding strength and accelerate the rupture of GKS.

For a specific temperature, interfacial bonding strength is the origin of reinforcement effect for nanocomposites. To provide the insights into the interfacial effect and load transfer patterns with respect to toughness and strength, we next investigate the interfacial bonding effect based on hybrid potential function. In the case of the maximum interfacial bonding strength, Tersoff potential is used to describe the interatomic interactions between Si and C, and for the interfacial bonding strength from 0.01 eV to 0.5 eV, we designate LJ potential function to simulate interactions of Si and C. And it can be written as $E^{LJ} = 4\epsilon [(r_{ij}/\sigma)^{-12} - (r_{ij}/\sigma)^{-6}]$, where ϵ is the energy scale parameter and represents the bonding strength, σ is the collision diameter parameter.

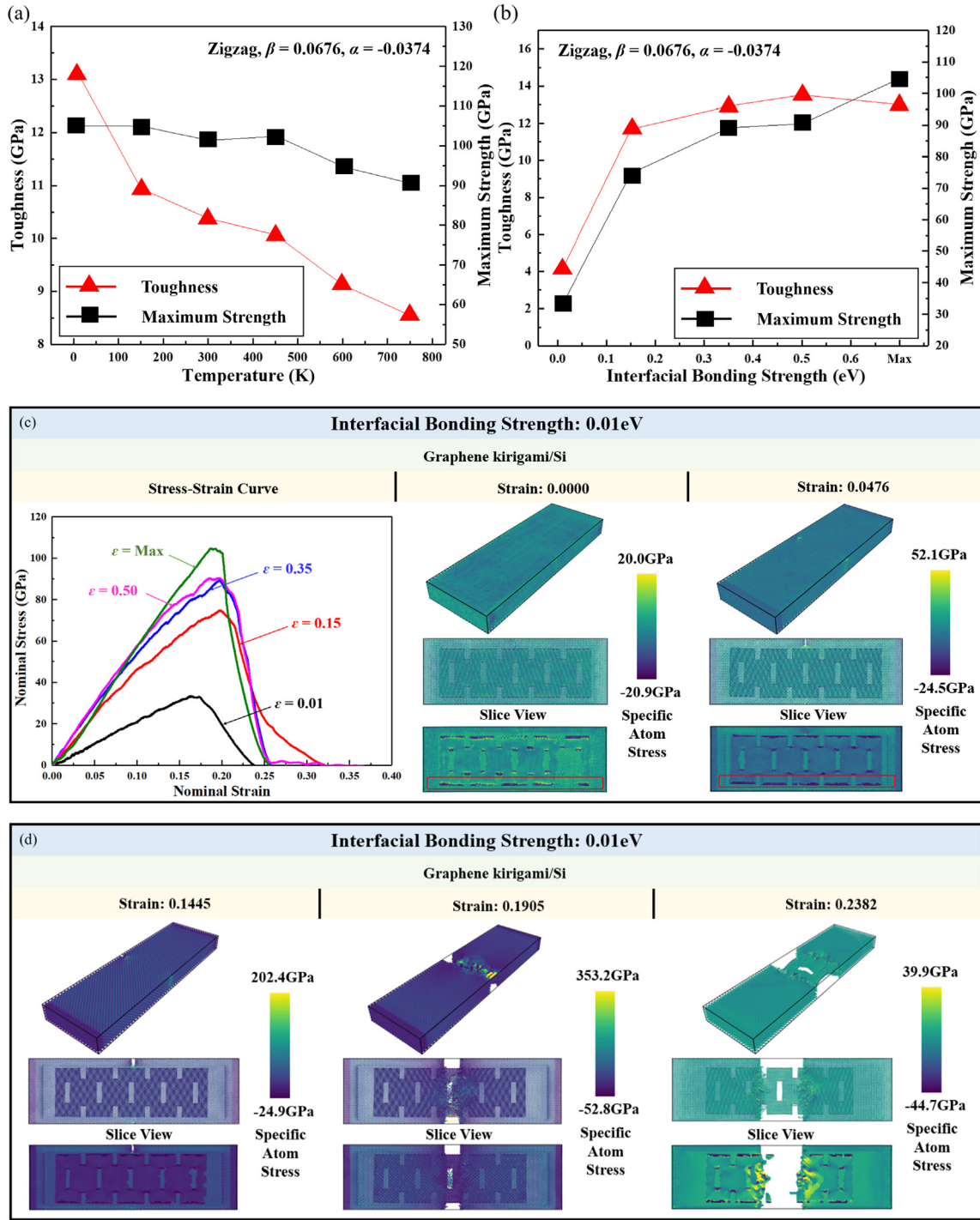


FIG. 4. (a) Temperature impact on toughness and maximum strength of GKSН with $\beta = 0.0676$ and $\alpha = -0.0374$ for zigzag graphene kirigami. (b) Effect of interfacial bonding strength on toughness and maximum strength of GKSН with $\beta = 0.0676$ and $\alpha = -0.0374$ for zigzag graphene kirigami. (c)–(d) Stress-strain for various interfacial bonding strength and snapshots of the deformation process for GKSН.

Fig. 4(b) shows the calculation results of the toughness and maximum strength for GKSН with various bonding strengths between C and Si. It is obvious that the calculated toughness and maximum strength increase with the increasing interfacial bonding strength at the interface of C and Si matrix in GKSН. For fully bonded GKSН, we find the toughness is slightly smaller than the interfacial bonding strength of 0.5 eV, the fact is that considerable defects will be formed on graphene surface after the initial equilibrium due to strong interatomic interaction of C and Si. In the case of the weakest bonding strength (0.01 eV), graphene kirigami as the reinforcement cannot function well and

enhance the mechanical properties of GKSН such as toughness and maximum strength, but it acts as a void in Si matrix and results in brittle fracture of Si material. To demonstrate the key mechanism, the snapshots of the weakest bonding case are specially captured as we can see in Fig. 4(c)–(d). Firstly, the stress-strain curves are displayed in the insert of Fig. 4(c), where the black line represents the weakest bonding strength (0.01 eV), and the calculated results of toughness and maximum strength are in line with Fig. 4(b). As shown in Fig. 4(c), the void will be formed after the initial equilibrium, and the voids grow with increasing of strain (see strain: 0.0000–0.0476–0.1445). From the strain

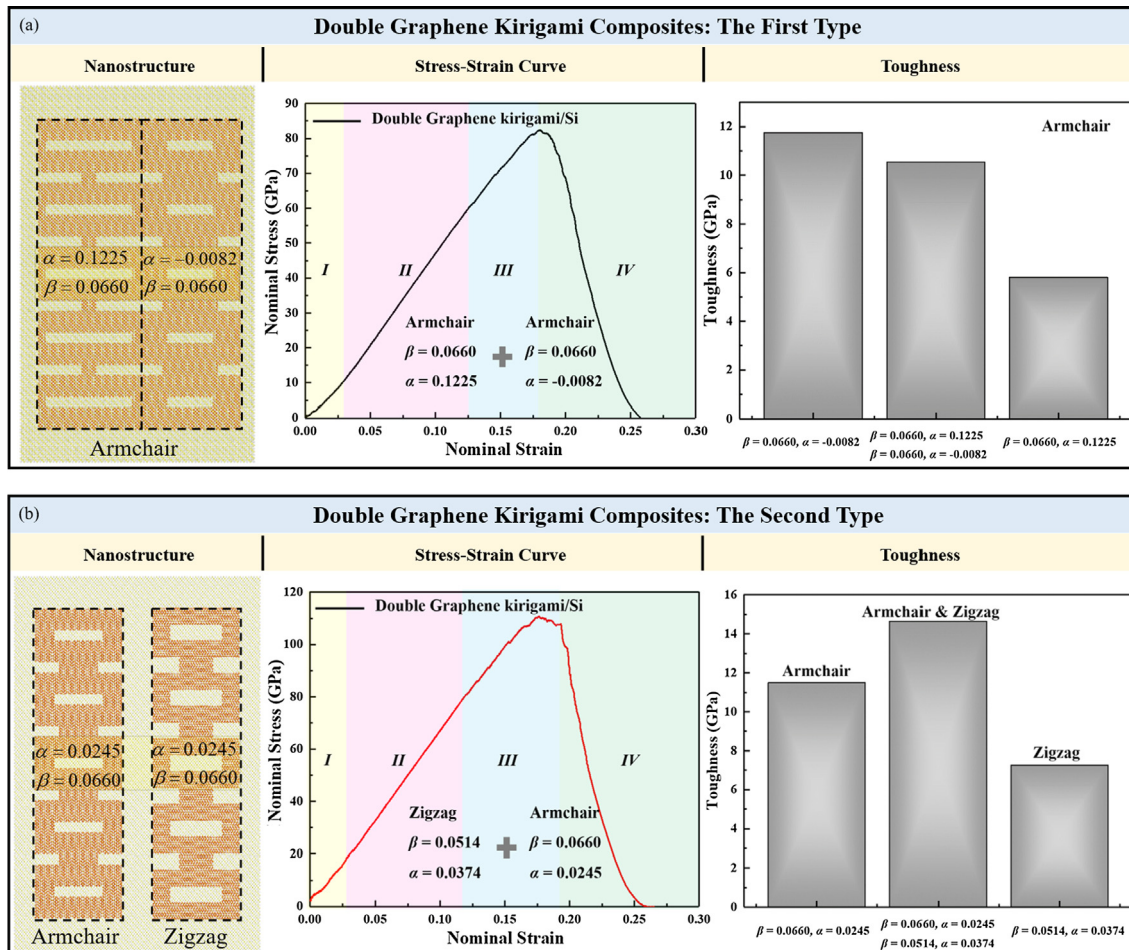


Fig. 5. Two typical double graphene kirigami embedded in Si matrix. (a) Model development and stress-strain curve for the first nanocomposite. The key geometry parameters of this configuration are made up of armchair graphene kirigami of $\alpha = -0.0082$, $\beta = 0.0660$ and armchair graphene kirigami of $\alpha = 0.1225$, $\beta = 0.0660$. (b) Model development and stress-strain curve for the second nanocomposite. The geometry parameters of this configuration are included by armchair graphene kirigami of $\alpha = 0.0245$, $\beta = 0.0660$ and zigzag graphene kirigami of $\alpha = 0.0374$, $\beta = 0.0514$. The space of two graphene kirigami is 31 Å.

of 0.1905 to 0.2382 (see Fig. 4(d)), the graphene kirigami is directly pulled out and it cannot contribute to load transfer between the Si-C interface. While the load transfer of Si-C interface will increase with increasing of the interfacial bonding strength as shown from Fig. 4(b).

3.4. Double graphene kirigami embedded in Si matrix

The efficiency of graphene kirigami in enhancing the toughness and maximum strength has been demonstrated, while based on the parametric analysis in Section 3.1 the novel GKS with a variable range of toughness, strength can be designed. The potential application of a single graphene kirigami embedded in nanocomposite is not our unique aim. Coupling use will develop the application scope. Before concluding, two typical double graphene kirigami embedded in Si matrix nanocomposites are proposed by previous investigations. As we can see from Fig. 5, the results for deformation response as shown in stress-strain curves are similar to a single of graphene kirigami. A more subtle design, ranging from toughness to strength, enabled by double use of kirigami graphene can advance the applicability of kirigami structure in nanocomposites. Especially, the toughness of the first type of novel nanocomposite is 10.55GPa as seen in Fig. 5(a), in which the value is between the single uses of GKSNs. While for the second type of novel nanocomposite the toughness can be further enhanced as we can see from Fig. 5(b). Such difference in terms of toughening effect can be strongly influenced by nanostructural symmetries in graphene kirigami composites. Locking effect due to geometric flipping and bridging

effects due to separated nanostructure of graphene kirigami in the second novel composite will be reinforced. There are still many aspects to be considered during the design, and the related design rules should be specified. The authors hope to answer this question in the near future.

4. Conclusion

In conclusion, MD results of the representative nanocomposite unit cell with tensile loading reveal that graphene kirigami is an effective method to enhance the toughness and strength of the silicon matrix composite, while silicon is a typical brittle material. Some conclusions are as follows.

- (1) The smaller α and the larger β will lead to the larger toughness, tensile modulus and maximum strength of GKS.
- (2) In stage I, competition relationships between wrinkling graphene kirigami and de-wrinkling effect induced by tensile loading can form a low slope of stress-strain curve.
- (3) In stage II, locking effect due to geometric flipping of graphene kirigami is main contribution of linear stress increasing, based on which the toughness and maximum strength of GKS can be larger than PGSN.
- (4) In stage III, breaking of local covalent bonds occurs. Bridging effects enable the maximum strength and toughness to increase finally in stage IV.

- (5) The load transfer can increase with increasing of the bonding strength. For weakest interfacial bonding, graphene kirigami can be directly pulled out.
- (6) Two novel double graphene kirigami embedded in Si matrix nanocomposites can be proposed, which accommodate the tendency of subtle controlling of mechanical properties of nanocomposites

CRediT authorship contribution statement

Yafei Wang: Conceptualization, Methodology, Software, Validation, Formal analysis, Investigation, Resources, Data curation, Writing - original draft, Writing - review & editing, Visualization, Supervision. **Changguo Wang:** Conceptualization, Methodology, Formal analysis, Investigation, Resources, Data curation, Writing - review & editing, Visualization, Supervision, Project administration, Funding acquisition. **Yunce Zhang:** Methodology, Software, Validation, Formal analysis, Investigation, Resources, Data curation, Visualization, Supervision. **Huifeng Tan:** Formal analysis, Resources, Data curation.

Acknowledgment

This work was supported by National Natural Science Foundation of China, 11572099; Natural Science Foundation of Heilongjiang Province of China, A2015002; the Fundamental Research Funds for the Central Universities, HIT.MKSTISP.2016_29; The Aeronautical Science Foundation of China, 2016ZA77001. The author would like to express his thanks and appreciation to the anonymous reviewers whose substantial and constructive comment significantly improved the research.

References

- [1] R. Zhao, S. Lin, H. Yuk, et al., Kirigami enhances film adhesion, *Soft Matter* 14 (2018) 2515–2525.
- [2] Y.S. Guan, Z. Zhang, Y. Tang, et al., Kirigami-inspired nanoconfined polymer conducting nanosheets with 2000% stretchability, *Adv. Mater.* 30 (2018) e1706390.
- [3] T.C. Shyu, P.F. Damasceno, P.M. Dodd, et al., A kirigami approach to engineering elasticity in nanocomposites through patterned defects, *Nat. Mater.* 14 (2015) 785–789.
- [4] Z. Wang, L. Zhang, S. Duan, et al., Kirigami-patterned highly stretchable conductors from flexible carbon nanotube-embedded polymer films, *J. Mater. Chem. C* 5 (2017) 8714–8722.
- [5] D. Akinwande, C.J. Brennan, J.S. Bunch, et al., A review on mechanics and mechanical properties of 2D materials-graphene and beyond, *Extr. Mech. Lett.* 13 (2017) 42–77.
- [6] T. Zhang, X. Li, H. Gao, Fracture of graphene: a review, *Int. J. Fract.* 196 (2015) 1–31.
- [7] S.F. Bartolucci, J. Paras, M.A. Rafiee, et al., Graphene-aluminum nanocomposites, *Mat. Sci. Eng. A-Struct.* 528 (2011) 7933–7937.
- [8] Y. Rong, H.P. He, L. Zhang, et al., Molecular dynamics studies on the strengthening mechanism of Al matrix composites reinforced by graphene nanoplatelets, *Comp. Mater. Sci.* 153 (2018) 48–56.
- [9] Z.G. Song, V.I. Artyukhov, J. Wu, et al., Defect-detriment to graphene strength is concealed by local probe: the topological and geometrical effects, *ACS Nano* 9 (2015) 401–408.
- [10] C. Wu, X. Wang, L. Lin, et al., ACS Nano, paper-based triboelectric nanogenerators made of stretchable interlocking kirigami patterns, 10 (2016) pp. 4652–4659.
- [11] Z. Yan, F. Zhang, J. Wang, et al., Controlled mechanical buckling for origami-inspired construction of 3D microstructures in advanced materials, *Adv. Funct. Mater.* 26 (2016) 2629–2639.
- [12] Z. Yan, M. Han, Y. Yang, et al., Controlled mechanical buckling for origami-inspired construction of 3D microstructures in advanced materials, *Extr. Mech. Lett.* 11 (2017) 96–104.
- [13] Y. Zhang, Z. Yan, K. Nan, et al., A mechanically driven form of Kirigami as a route to 3D mesostructures in micro/nanomembranes, *PNAS* 112 (2015) 11757–11764.
- [14] J. Lyu, M.D. Hammig, L. Liu, et al., Stretchable conductors by kirigami patterning of aramid-silver nanocomposites with zero conductance gradient, *Appl. Phys. Lett.* 111 (2017) 161901.
- [15] L. Xu, X. Wang, Y. Kim, et al., Kirigami nanocomposites as wide-angle diffraction gratings, *ACS Nano* 10 (2016) 6156–6162.
- [16] J. Cho, A.R. Boccaccini, M.S.P. Shaffer, Ceramic matrix composites containing carbon nanotubes, *J. Mater. Sci.* 44 (2009) 1934–1951.
- [17] J. Cho, F. Inam, M.J. Reece, et al., Carbon nanotubes: do they toughen brittle matrices? *J. Mater. Sci.* 46 (2011) 4770–4779.
- [18] J. Ning, J. Zhang, Y. Pan, J. Guo, Fabrication and mechanical properties of SiO₂ matrix composites reinforced by carbon nanotube, *Mat. Sci. Eng. A-Struct.* 357 (2003) 392–396.
- [19] S. Guo, R. Sivakumar, H. Kitazawa, et al., Electrical properties of silica-based nanocomposites with multiwall carbon nanotubes, *J. Am. Ceram. Soc.* 90 (2007) 1667–1670.
- [20] R. Sivakumar, S. Guo, T. Nishimura, et al., Thermal conductivity in multi-wall carbon nanotube/silica-based nanocomposites, *Scr. Mater.* 56 (2007) 265–268.
- [21] H. Chen, S. Chen, The fracture behaviors of carbon nanotube and nanoscroll reinforced silicon matrix composites, *Carbon* 67 (2014) 344–351.
- [22] C. Lee, X. Wei, J.W. Kysar, et al., Ultrahard nanotwinned cubic boron nitride, *Science* 321 (2008) 385–388.
- [23] M.K. Blees, A.W. Barnard, P.A. Rose, et al., Graphene kirigami, *Nature* 524 (2015) 204.
- [24] B. Mortazavi, A. Lherbier, Z. Fan, et al., Thermal and electronic transport characteristics of highly stretchable graphene kirigami, *Nanoscale* 9 (2017) 16329–16341.
- [25] D.A. Bahamon, Z. Qi, H.S. Park, et al., Graphene kirigami as a platform for stretchable and tunable quantum dot arrays, *Phys. Rev. B* 93 (2016).
- [26] Z. Qi, D.K. Campbell, H.S. Park, Atomistic simulations of tension-induced large deformation and stretchability in graphene kirigami, *Phys. Rev. B* 90 (2014).
- [27] S. Plimpton, Fast parallel algorithms for short-range molecular-dynamics, *J. Comput. Phys.* 117 (1995) 1–19.
- [28] F. Pavia, W.A. Curtin, Interfacial sliding in carbon nanotube/diamond matrix composites, *Acta Mater.* 59 (2011) 6700–6709.
- [29] S.J. Chen, C.Y. Li, Q. Wang, et al., Reinforcing mechanism of graphene at atomic level: Friction, crack surface adhesion and 2D geometry, *Carbon* 114 (2017) 557–565.
- [30] P. Erhart, K. Albe, Analytical potential for atomistic simulations of silicon, carbon, and silicon carbide, *Phys. Rev. B* 71 (2005).
- [31] W.G. Jiang, Y. Wu, Q.H. Qin, et al., A molecular dynamics based cohesive zone model for predicting interfacial properties between graphene coating and aluminum, *Comp. Mater. Sci.* 151 (2018) 117–123.
- [32] R. Rezaei, Tensile mechanical characteristics and deformation mechanism of metal-graphene nanolayered composites, *Comp. Mater. Sci.* 151 (2018) 181–188.
- [33] H.Y. Song, X.W. Zha, Influence of nickel coating on the interfacial bonding characteristics of carbon nanotube–aluminum composites, *Comp. Mater. Sci.* 49 (2010) 899–903.
- [34] B.H. Kim, K.R. Lee, Y.C. Chung, et al., Effects of interfacial bonding in the Si-carbon nanotube nanocomposite: a molecular dynamics approach, *J. Appl. Phys.* 112 (2012) 044312.
- [35] S.J. Stuart, A.B. Tutein, J.A. Harrison, A reactive potential for hydrocarbons with intermolecular interactions, *J. Chem. Phys.* 122 (2000) 6472–6486.
- [36] D.W. Brenner, O.A. Shenderova, J.A. Harrison, et al., A second-generation reactive empirical bond order (REBO) potential energy expression for hydrocarbons, *J. Phys. Condens. Mat.* 14 (2002) 783–802.
- [37] B. Morris, M. Becton, X. Wang, Mechanical abnormality in graphene-based lamellar superstructures, *Carbon* 137 (2018) 196–206.
- [38] L.S. Walker, V.R. Marotto, M.A. Rafiee, et al., Toughening in graphene ceramic composites, *ACS Nano* 5 (2011) 3182–3190.
- [39] K.E. Petersen, Silicon as a mechanical material, *Proc. IEEE* 76 (5) (1982) 420–457.